Featured in Physics

Rapid Evolution of the Photosystem II Electronic Structure during Water Splitting

Katherine M. Davis,[1,†] Brendan T. Sullivan,[1,‡] Mark C. Palenik,[1,§] Lifen Yan,[1] Vatsal Purohit,[1,¶] Gregory Robison,[1,‖] Irina Kosheleva,[2] Robert W. Henning,[2] Gerald T. Seidler,[3] and Yulia Pushkar[1,*]

[1]*Department of Physics and Astronomy, Purdue University, West Lafayette, Indiana 47907, USA*
[2]*Center for Advanced Radiation Sources, The University of Chicago, Chicago, Illinois 60637, USA*
[3]*Department of Physics, University of Washington, Seattle, Washington 98195, USA*

(Received 10 May 2018; revised manuscript received 18 July 2018; published 23 October 2018)

Photosynthetic water oxidation is a fundamental process that sustains the biosphere. A Mn_4Ca cluster embedded in the photosystem II protein environment is responsible for the production of atmospheric oxygen. Here, time-resolved x-ray emission spectroscopy (XES) is used to observe the process of oxygen formation in real time. These experiments reveal that the oxygen evolution step, initiated by three sequential laser flashes, is accompanied by rapid (within 50 μs) changes to the Mn $K\beta$ XES spectrum. However, no oxidation of the Mn_4Ca core above the all-Mn^{IV} state is detected to precede O—O bond formation, and the observed changes are therefore assigned to O—O bond-formation dynamics. We propose that O—O bond formation occurs prior to the transfer of the final (fourth) electron from the Mn_4Ca cluster to the oxidized tyrosine Tyr_Z residue. This model resolves the kinetic limitations associated with O—O bond formation and suggests an evolutionary adaptation to avoid releasing harmful peroxide species.

DOI: 10.1103/PhysRevX.8.041014 Subject Areas: Biological Physics

Enzymes function as nature's catalysts, facilitating virtually all the reactions necessary for life. By carefully coordinating electron dynamics and atomic rearrangements within a predefined energy landscape, they enable a broad range of efficient and highly selective transformations, many of which have proven challenging for chemists. Among these, the reaction catalyzed by the Mn_4Ca cluster of photosystem II (PS II) during photosynthesis holds a special place, as the ability to biosynthesize O_2 from H_2O occurred only once during evolution. The development of this process dramatically altered our planet by generating the oxygen-rich atmosphere we live in today. The catalytic activity and quantum efficiency of the oxygen evolving complex (OEC) remain unmatched by synthetic systems developed for artificial photosynthesis. Despite its far-reaching consequences, the underlying mechanism of PS II remains debated.

In 1970, Kok, Forbush, and McGloin described a potential water-splitting mechanism in which the OEC cycles through five states (S_0–S_4), corresponding to the oxidation states of manganese, following sequential visible-light absorptions [Fig. 1(a)] [1]. Antenna pigments from the surrounding protein matrix absorb these photons and funnel energy towards P_{680}, the chlorophyll *a* special pair responsible for charge separation. Within nanoseconds, the tyrosine residue (Tyr_Z) located between P_{680} and the OEC is oxidized by the special pair to form $Tyr_Z^{\bullet}$, which is subsequently reduced by the OEC on a microsecond timescale. This process drives the water-splitting reaction [2].

The past 40 years have yielded new insights into the structure of PS II [6–15], as well as the nature and timing of the *S*-state transitions that form the Kok cycle [Fig. 1(a)] [3,16–19]. Nonetheless, the critical step during which the O—O bond is formed remains poorly characterized and, thus, cannot be implemented in artificial systems. O—O bond formation likely occurs on a microsecond timescale during the S_3-to-S_0 transient step of the catalytic cycle, culminating in O_2 evolution. Direct monitoring of this transient process, however, has proven challenging, and details remain elusive. A preeminent report by Babcock, Blankenship, and Sauer, as well as recent studies by Nilsson *et al.*, support a rate of $Tyr_Z^{\bullet}$ reduction with $t_{1/2} \sim 1$ ms following three flashes and associates this rate

*Corresponding author.
ypushkar@purdue.edu
†Present address: Department of Chemistry, Princeton University, Princeton, NJ 08544, USA.
‡Present address: Neutron Scattering Division, Oak Ridge National Laboratory, Oak Ridge, TN 37830, USA.
§Present address: Naval Research Laboratory, Washington, DC 20375, USA.
¶Present address: Department of Biology, Purdue University, West Lafayette, IN 47907, USA.
‖Present address: Department of Physics and Astronomy, Hanover College, Hanover, IN 47243, USA.

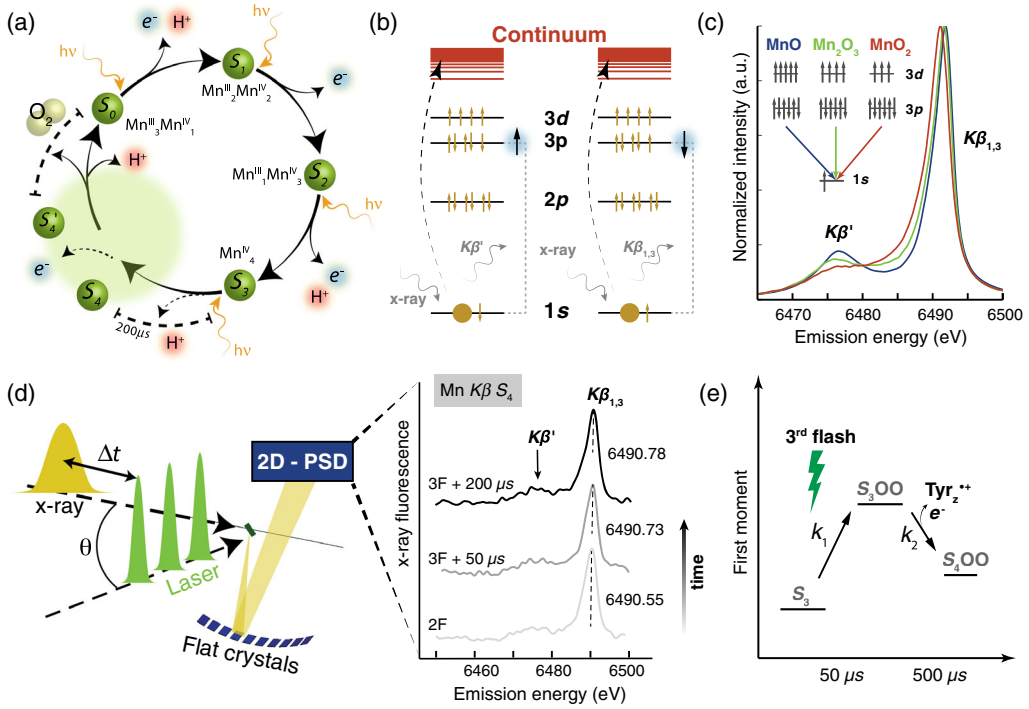

FIG. 1. (a) Current model of the Kok cycle. Depiction of sequential incident visible-light photon absorptions triggering electron or proton release [3]. The dashed region is based on previous analysis of the S_3-to-S_0 transition in which the S_4 state is proposed [3,4]. (b) Electronic transitions, reflected in the $K\beta$ main lines, are influenced by the spin state of the Mn ion. (c) A spectral comparison of Mn oxides depicts the effect of oxidation state on the $K\beta$ emission lines. (d) Nanosecond laser pulses (1, 2, or 3) are used to advance the Kok cycle in the protein (Table S1 [5]). The pump-probe delay time Δt, measured from the final laser flash to the center of the x-ray pulse, is set dependent on the desired S state. X-ray fluorescence from the sample is reflected by ten flat analyzer crystals onto a 2D-position-sensitive detector. $K\beta$ emission spectra are extracted to form snapshots of the electronic structure in time. Smoothed emission spectra are presented for $2F$ (majority S_3) and two time points during the S_3-to-S_0 transition. (e) The proposed reaction scheme shows the early evolution of the OEC during the S_3-to-S_0 transition, providing an interpretation of spectroscopic results.

constant with the formation of the S_4 state, subsequently capable of fast O_2 evolution [20,21]. It was pointed out later that such hypotheses face a serious kinetic challenge in that the timescale of molecular oxygen release, following the formation of the S_4 state, is very short for the associated redox chemistry and bond-formation dynamics [22]. As an alternative hypothesis, S_3-state peroxide formation was proposed [22], but this proposal has not yet been confirmed experimentally.

Given the lack of definitive spectroscopic results, computational simulations have been performed to model the O—O bond-formation path [23–26]. Many of these imply oxidation of the OEC past $Mn^{IV}{}_4$ via the formation of a $Mn^{V}Mn^{IV}{}_3$ state, also presented as $Mn^{IV}{}_4 - O^{\bullet}$ (oxyl radical). This oxidized configuration is currently associated with S_4 and would precede O—O bond formation [23,27]. Experimental proof for a $Mn^{V}Mn^{IV}{}_3$ intermediate state is currently lacking, and our data rule out its formation. Here, we examine the earliest dynamic in the S_3-to-S_0 transition via time-resolved x-ray emission spectroscopy (TR XES), utilizing dispersive detection, to aid our understanding of this critical biological process [28,29]. In 2015, we proposed a new mechanistic model [Fig. 1(e)] in which O—O bond formation occurs prior to the transfer of the final (fourth) electron from the Mn_4Ca cluster to explain our preliminary spectroscopic results [30]. An x-ray crystallographic study of the S_3 state [13] recently confirmed our DFT-based proposal, producing a virtually indistinguishable S_3-state model, within the experimental resolution of x-ray diffraction [31].

Here, we deliver an extensive statistical analysis of these initial data sets in conjunction with those collected subsequently, each consistently composed of almost a half million repetitive interrogations of the OEC electronic structure. The power of large statistical data sets has long been realized, often enabling the development of new research tools. A single, blurry electron microscopy image of a complex biomolecule, for instance, provides little insight into its structure, while several thousand images can now deliver atomically resolved models [32]. In a similar fashion, repetitive measurement of a spectroscopic response allows us to solidify the rapid electronic structure evolution in the S_3-to-S_0 transition, a result which is

TABLE I. Experimental characteristics of the pulsed x-ray source.

Characteristics	BioCARS
Excitation energy	Peak energy 7.85 keV, FWHM about 500 eV
X-ray spot size	Approximately 45×100 μm^2
Pulse length	44 μs (22 μs data set 5)
Photon flux	3×10^{11} photons/pulse
Dose delivered per pulse	Approximately 7×10^7 photons/μm^2

required to complete the description of O—O bond formation in natural photosynthesis.

Mn $K\beta$ spectral emission lines reflect the number of unpaired $3d$ electrons and, thus, provide information about the oxidation and/or spin states for a given Mn ion, inaccessible via structural methods such as x-ray crystallography [33]. The exchange interaction between the $3p$ hole and $3d$ valence electrons in the final state causes multiplet splitting that results in separate $K\beta_{1,3}$ and $K\beta'$ peaks [Figs. 1(b) and 1(c)]. This coupling is directly linked to the electronic state of Mn such that an increase in the oxidation state results in decreased splitting between the $K\beta$ spectral lines. This effect is most apparent in the $K\beta_{1,3}$ peak position shift to lower energies with increasing oxidation. XES also allows for dispersive detection, in which the full emission spectrum is recorded during a single, intense, polychromatic x-ray pulse [Fig. 1(d)] [28]. The temporal resolution of such a setup is limited in practice only by the time structure of the x-ray source. In our experiments, we utilize multibunch x-ray exposures of 22–44 μs duration to match the microsecond kinetics of the OEC [3] [Table I and Fig. S1(a) [5]]. We previously determined that exposures of up to 66 μs under these conditions are undamaging to PS II [28,34]. Data collection is performed using a von Hamos–style miniature x-ray emission spectrometer (miniXES) [Fig. S1(b) [5]] [28,35], and a nonjet open-air sample delivery system [see Supplemental Material and Fig. S1(c) [5]] is used to supply fresh, unrecycled PS II for each measurement at a controlled repetition rate. Samples are excited given a defined number (0–3) of laser flashes (F) and probed at a time (Δt) after the final laser flash by a single x-ray pulse [Figs. 1(d) and S1(a) and Table S1 [5]]. For clarity, we note that $0F$, i.e. no laser flashes, corresponds to majority state S_1, $1F$ corresponds to majority state S_2, etc.

Our total data set is composed of five separate beam times, ultimately accumulating over two million x-ray pulses to measure different S states (Table II). Note that data set five is analyzed separately as its background differs from the other four beamtimes due to beamline upgrades. Time-resolved spectra of the majority S states S_1, S_2, and S_3 are collected following zero, one, and two laser flashes, respectively, with a spacing between consecutive laser flashes of 100 ms, corresponding to a laser frequency of 10 Hz. Samples are probed with the x-ray beam following a $\Delta t = 500$ μs time delay from the final laser flash to allow for the full reduction of $Tyr_Z^{\bullet}$ with limited decay of the formed S state (Table S1 [5]) [3,36]. Given the multiplet character of the spectra and the noise inherent for such a dilute biological sample, previous studies recommend the use of the statistical first moment $(\sum_j E_j \cdot I_j)/(\sum_j I_j)$, surrounding the $K\beta_{1,3}$ peak, as an indicator of changes to the electronic structure (Figs. 2 and 3) [37]. It has been reported, and should be emphasized here, that *any* data manipulation such as background subtraction and smoothing can affect first moment magnitudes, leading to a risk of misinterpretation of small spectral changes [19]. To avoid uncertainties due to these processing methods, we provide the first-ever analysis of primary photosystem II emission data. These data sets are subject to no manipulation beyond the extraction of spectra via energy calibration of the detector. The statistical significance of the observed spectral changes is then determined using

TABLE II. Approximate number of x-ray pulses per state, per beam time.

		Data sets				
Majority S state	Flash	1	2	3[a]	4	5[b]
S_0	$3F_{40\ ms}$	43 250	60 000	55 333	107 222	97 800
S_1	0	62 267	72 800	60 233	n/a	100 000
S_2	1	42 083	61 556	55 333	n/a	88 900
S_3	2	n/a	62 000	57 178 48 889	107 222	95 600
S_{4a}	$3F_{50\ \mu s}$	n/a	n/a	57 178 48 889	111 667	93 300
S_{4b}	$3F_{200\ \mu s}$	n/a	60 889	57 178 48 889	110 556	86 700
S'_4	$3F_{500\ \mu s}$	43 750	60 889	57 400	n/a	91 100
Total		191 350	322 334	546 500	436 667	653 400

[a]Additional statistics are collected for S_3, S_{4a}, and S_{4b} for data set 3. The columns are split to reflect the additional x-ray pulses for these states.

[b]This data set is collected after 2015 upgrades to the optics at the BioCARS beam line which made impossible the use of the old experimental conditions and required twice shorter (1/2 intensity) pulses to minimize the heat load on new optics components.

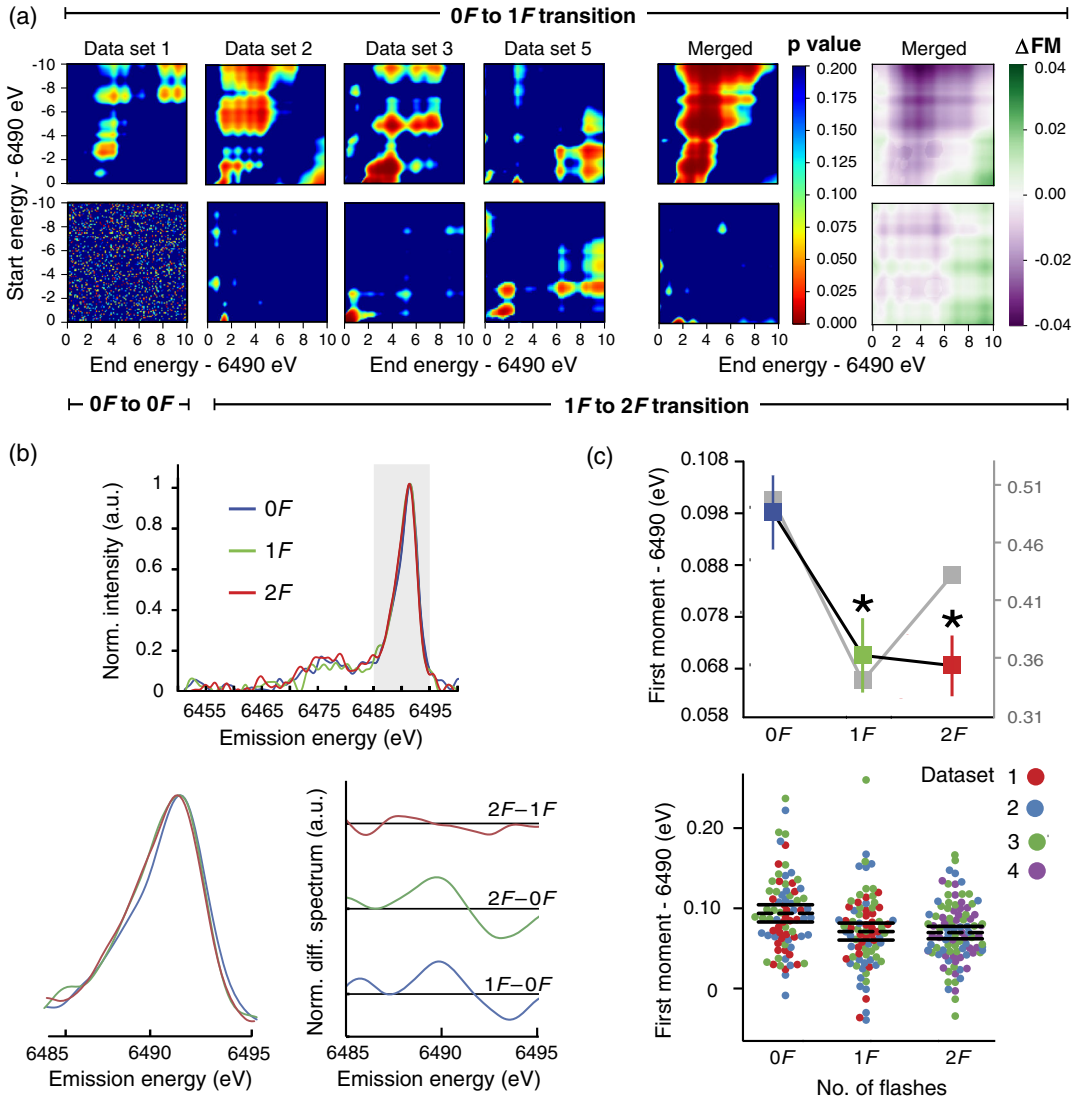

FIG. 2. Analysis of the statistical significance for $S_1 \rightarrow S_2 \rightarrow S_3$ transitions serves as a proof of concept. (a) Spectral shifts occurring as a result of $0F \rightarrow 1F$ and $1F \rightarrow 2F$ transitions are characterized using 2D heat maps, illustrating the p value (see Table S2 for n [5]) for changes to first moments calculated over the ranges defined by the x and y axes, i.e., start and end energy, respectively. Contours appear in plots comparing $0F \rightarrow 1F$ data indicate a statistically significant difference. By contrast, limited low p-value regions are observed for the $1F \rightarrow 2F$ transition, suggesting a smaller change. The directionality and magnitude of spectral shifts are shown in the final column. These 2D heat maps, which graphically illustrate the change in first moments ($\Delta\text{FM} = \text{FM}_{\text{postflash}} - \text{FM}_{\text{preflash}}$) calculated over the ranges defined by the x and y axes. $0F \rightarrow 1F$ and $1F \rightarrow 2F$ transitions are dominated by negative, or oxidative, shifts. An example of statistical noise is presented by randomly dividing a $0F$ data set and performing the same analysis, e.g., $0F \rightarrow 0F$. Relevant data from data sets 1–4 are merged to generate the final columns. Note that $0F$ and $1F$ data are not collected for data set 4, while data set 5 is collected independently following a beam-line upgrade and is therefore analyzed separately; see Fig. S4 [5]. (b) Wavelet-transform smoothed and background-subtracted emission spectra for merged $0F$, $1F$, and $2F$ data. The region (6.485–6.495 keV), over which the first moment is calculated, is highlighted, and a magnified inset as well as difference spectra are presented. Difference spectra are smoothed with a rolling average calculated over 14 points (approximately ±0.7 eV). (c) (Top) Average first moments from unprocessed (color) and processed (gray) spectra. Errors are presented as SEM with n given in Table III. Those moments with a statistically significant difference ($p < 0.05$) from $0F$ data are indicated with an asterisk. (Bottom) Dot plot of first moments from raw data. Each dot represents a calculated first moment from a thread collected during the beam time corresponding to its color in the legend. Dashed lines represent the average first moment, while solid bars are the 95% confidence interval.

one-way analysis of variance (ANOVA), a simple statistical method employed broadly across many scientific disciplines. Resultant p values represent the probability of falsely rejecting the null hypothesis, i.e., that a difference in the first moment between the two states listed is a random statistical variation. Thus, the lower the p value, the stronger the evidence for changes in the spectra between compared data sets. In this study, we take the

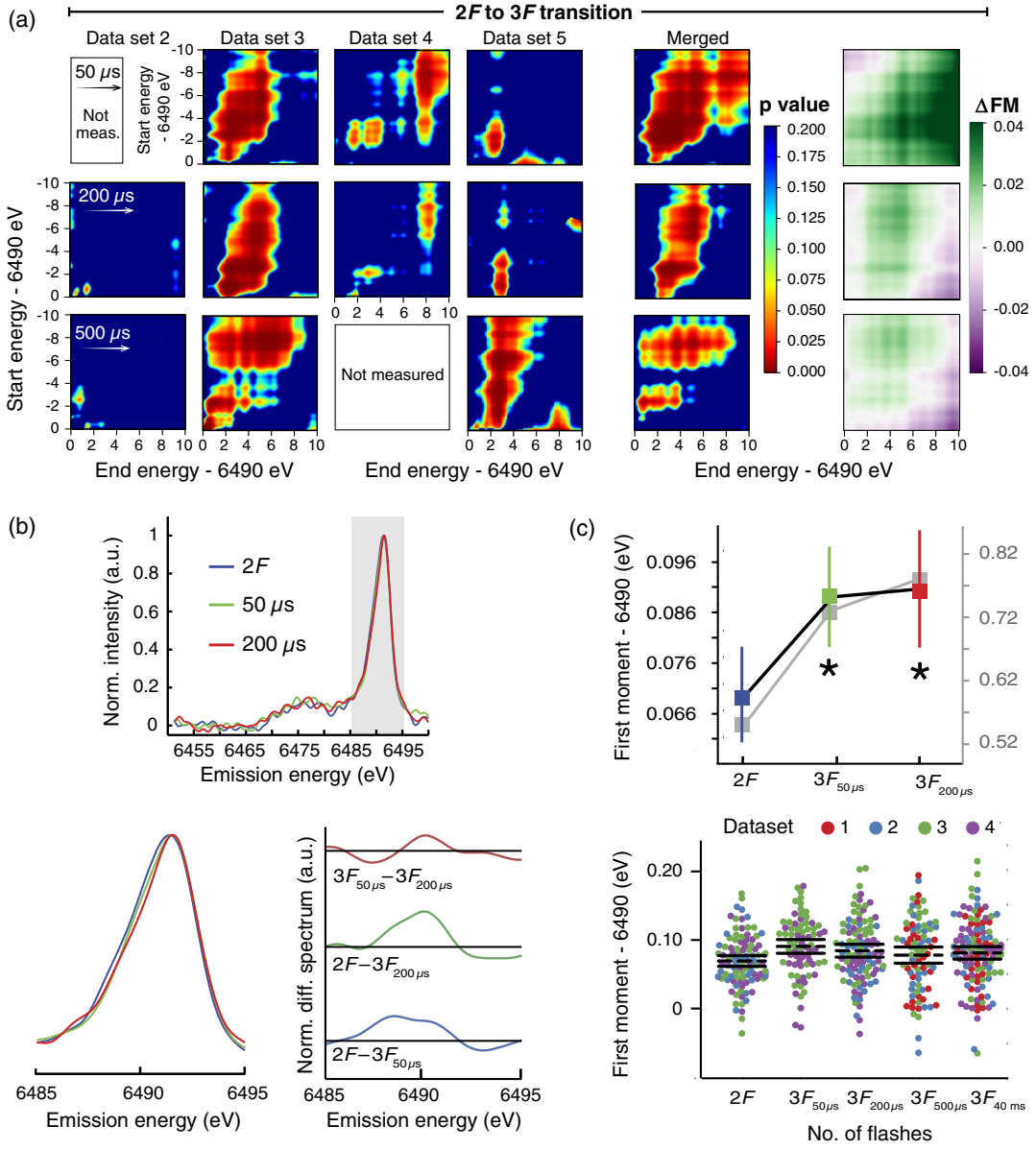

FIG. 3. Rapid onset of spectral changes observed during the S_3-to-S_0 transition. (a) Spectral shifts occurring as a result of the $2F \rightarrow 3F$ transition are characterized using 2D heat maps colored by p value (see Table S2 [5] for n), for changes to first moments calculated over the ranges defined by the x and y axes, i.e., start and end energy, respectively. Strong contours are consistently observed, indicative of a statistically significant spectral change. The directionality and magnitude of spectral shifts occurring with these transitions are also shown as 2D heat maps, which graphically illustrate the change in first moments ($\Delta\text{FM} = \text{FM}_{\text{postflash}} - \text{FM}_{\text{preflash}}$) calculated over the ranges defined by the x and y axes. All $2F \rightarrow 3F$ comparisons yield primarily positive, or reductive, shifts. Determined p values of approximately 0.02 (Table III) for the 200 μs time point are further supported by the above heat maps; however, little information can be gleaned from these plots of data set 2, likely due to much lower x-ray shot count; see Table II. Although the 500 μs time point is equally compelling, the traditional energy range (6.485–6.495 keV) selected for reporting first moments does not deliver statistical significance (Table III). (b) Wavelet transform smoothed and background-subtracted emission spectra for merged $2F$, $3F_{50\ \mu s}$, and $3F_{200\ \mu s}$ data, calculated as in Fig. 2(b). (c) (Top) Average first moments from unprocessed (color) and processed (gray) spectra. Errors are presented as SEM with n given in Table III. Those moments with a statistically significant difference ($p < 0.05$) from $2F$ data are indicated with an asterisk. (Bottom) Dot plot of first moments from raw data, presented as in Fig. 2(c). See Fig. S3 [5] for 2D plots of the 40 ms (majority S_0 state) time point.

95% confidence interval to be significant. Background subtraction and smoothing are used only to produce figures for comparison with previous XES PS II studies, which all present significantly processed data.

While it is common to analyze first moments calculated over 6485–6495 eV, this approach fails to convey the full information content of XES spectra. To show that our trends are not dependent on a particular range chosen for

analysis of the first moment, p contours over variable energy integration ranges are shown in Figs. 2, 3, and S3 [5]. It is evident that merged data are dominated by statistically significant shifts, with the exception of $1F$ to $2F$, in agreement with earlier work [37]. Note that corners of the contour maps, which encompass either integration ranges outside the peak position or incomplete portions of the peak, may be influenced more significantly by noise, which is especially true for contour maps of individual beam times.

S_1-to-S_2 state transition.—The obtained S_1 state spectral shape and peak position are in good agreement with previous RT PS II measurements [28]. A comparison of $0F$ and $1F$ first moments evaluated by one-way ANOVA shows a reproducible, statistically significant shift of the $K\beta_{1,3}$ peak to lower energies (Table III and Figs. 2 and S4 [5]). Cryogenic measurements previously reported a −0.059 eV shift following spectral smoothing and background subtraction procedures [37]. Analysis of three combined data sets (1, 2, and 3) following similar data processing yields a first moment shift of −0.16 eV for our $0F \rightarrow 1F$ transition (note that data set 4 is measured without the S_2 state, and 5 is measured after the beamline update and analyzed separately). The observed shift of the $K\beta_{1,3}$ peak to lower energies following a single laser flash is likewise consistent with previous cryogenic XANES [11,38] and recently published room-temperature XES [19] results for the S_1-to-S_2 state transition, both of which indicate Mn-centered oxidation. X-ray free electron laser (XFEL)-based TR XES experiments struggle to reproduce this result, likely due to a combination of lower spectrometer resolution and data-processing methods [29]. Although some XFEL studies [39,40] observe spectral shifts for x-ray measurements made following a different number of laser flashes, they have not yet provided any new mechanistic insights. Overall, we consider our results for the $0F \rightarrow 1F$ transition robust and in good agreement with the previous characterization of the S_1-to-S_2 transition in which one Mn center is oxidized from Mn^{III} to Mn^{IV}.

S_2-to-S_3 state transition.—For the ensuing S-state transition, $S_2 \rightarrow S_3$, previous cryogenic measurements determined that changes to the Mn $K\beta$ emission spectrum are minimal, and a small (−0.02 eV) shift, on the order of our systematic error (0.02 eV; see Supplemental Material [5] for more details), is reported [37]. A comparison of our $1F$ and $2F$ first moments, analyzed with one-way ANOVA, indicates a lack of statistical significance over most energy ranges (Table III and Figs. 2 and S4 [5]). Any associated spectral differences are likely too small to reach statistical significance under our experimental conditions. In contrast to both these measurements and earlier XAS studies [11,34,35], Zaharieva *et al.* recently observed a shift in the room-temperature emission spectrum equivalent to that observed during the $S_1 \rightarrow S_2$ transition [19]. Although the proposed Mn oxidation to form $Mn^{IV}{}_4$ in the S_3 state [41–45] [Fig. 1(a)], at its most basic, suggests a comparable XES shift for $S_1 \rightarrow S_2$ and $S_2 \rightarrow S_3$ transitions, we now know that the OEC undergoes a major structural change during the $S_2 \rightarrow S_3$ transition from both extended x-ray fine structure (EXAFS) [38], femtosecond (fs) x-ray crystallography [12–14], and electron paramagnetic resonance (EPR) [44]. Studies on model compounds indicate that changes to the local spin densities associated with structural rearrangements, such as changes to the ligand environment, could obscure a Mn-centered oxidative shift [31,46,47]. Minimal changes to the emission spectra, observed upon the $S_2 \rightarrow S_3$ transition in previous studies, are attributed to ligand-centered oxidation [37]. Low S_1-to-S_2 state conversion following the first laser flash could produce equivalent changes in the S_1-to-S_2 and S_2-to-S_3 transitions observed by Zaharieva, Dau, and Haumann [18]; however, the origin of such discrepancies between reports has yet to be elucidated.

S_0 forms after O_2 evolution.—To probe samples enriched with S_0, XES spectra are collected after a 40-ms delay following a third laser flash ($3F_{40\ \mathrm{ms}}$). The first moment of $3F_{40\ \mathrm{ms}}$ is consistently shifted to higher

TABLE III. p and F-statistic values from ANOVA for state-to-state comparisons between the state in the row and the state in the column for data sets 1–4 combined. p values are based on the first moments over the range 6.485–6.495 keV. The number of "samples" (i.e., threads) is shown in parentheses for each state. These values are broken down by beam time in Table S2 [5]. See Table II for additional comparisons between the states based on the number of x-ray pulses per state per beam time and Figs. 2(c) and 3(c) for dot plots of all first moments used for p-value calculations. Values for the F-statistic are given in parentheses. An analysis of data set 5 is shown in Fig. S4 [5].

		S_0	S_1	S_2	S_3	S_{4a}	S_{4b}	S'_4
Majority S state (n)	Flash	$3F_{40\ \mathrm{ms}}$	$0F$	$1F$	$2F$	$3F_{50\ \mu\mathrm{s}}$	$3F_{200\ \mu\mathrm{s}}$	$3F_{500\ \mu\mathrm{s}}$
S_0 (117)	$3F_{40\ \mathrm{ms}}$	1	0.08 (3.06)	0.06 (2.19)	0.06 (3.60)	0.17 (1.82)	0.63 (0.23)	0.66 (0.19)
S_1 (78)	$0F$		1	<0.01 (9.00)	<0.01 (13.56)	0.68 (0.17)	0.19 (1.67)	0.05 (3.80)
S_2 (81)	$1F$			1	0.85 (0.04)	<0.01 (7.27)	0.02 (3.68)	0.98 (0.82)
S_3 (96)	$2F$				1	<0.01 (11.32)	0.02 (5.87)	0.22 (1.50)
S_{4a} (75)	$3F_{50\ \mu\mathrm{s}}$					1	0.11 (0.80)	0.18 (2.60)
S_{4b} (98)	$3F_{200\ \mu\mathrm{s}}$						1	0.39 (0.73)
S'_4 (82)	$3F_{500\ \mu\mathrm{s}}$							1

energies [Figs. 3(c), S3, and S4 [5]], supporting the expected reduction of Mn. Overall, the RT TR XES results are in good agreement with previous Mn $K\beta$ emission data [19,37]. Having validated the experimental technique, we investigate the elusive transient S_3-to-S_0 process also initiated by three laser flashes ($3F$).

O—O *bond formation step*.—Figure 3 depicts the earliest evolution of the OEC electronic structure following three laser flashes and the associated first moment changes of Mn $K\beta_{1,3}$ measured at $\Delta t \sim 50$ μs ($3F_{50\ \mu s}$) and $\Delta t \sim 200$ μs ($3F_{200\ \mu s}$). The trend of an increasing first moment is robust and statistically significant (Table III and Figs. 3 and S4 [5]). It is important to note that this statistically significant change occurs after the S_2-to-S_3 transition, for which our analysis does *not* detect a statistically significant change in the spectra (Table 3 and Fig. 2). Furthermore, the observed increase in the first moment cannot be explained by mixing of S states due to poor protein advancement, as this mixing would produce an oxidative (decrease in the first moment) trend or no change; see Supplemental Material [5] for details regarding laser excitation. Based on the results of our statistical analysis, there is less than a 5% chance that this trend of an increasing first moment is merely noise. It is extremely unlikely that we would repeatedly observe p values less than 0.05 if we were prevented from detecting small spectral changes due to inherent limitations of our spectroscopic setup. Random reassignment of S-state labels, representative of data sets limited by spectrometer resolution, for example, yields p values less than 0.05 in only 5% of the random assignments, which is the expected false-positive rate. We are therefore confident that these trends are not resolution limited. To further probe the robustness of the shifts, we repeat our ANOVA analysis on randomly divided halves of the data. Recovery of statistical significance after this procedure demonstrates that there is, in fact, a $(5\%)^2 = 0.25\%$ chance that the reported effect is due to noise.

This statistically significant spectral shift suggests that during the S_3-to-S_0 transition the OEC undergoes a significant transformation at short timescales. Changes observed at 50 and 200 μs are likely due to a short-lived isoform of the S_3 state (S_3OO), in which the O—O bond has been formed and Mn centers have been reduced from the $(Mn^{IV})_4$ state [48]. The accumulation of this species is controlled by its rate of formation (k_1) and rate of oxidation due to electron transfer to $Tyr_Z^\bullet$ (k_2), which produces a one-electron-more oxidized S_4OO state [Fig. 1(e)]. The first moment of the Mn $K\beta_{1,3}$ line is commonly correlated with the nominal spin value of the Mn center (Fig. 4). We observe that the nominal spin of $3F_{50\ \mu s}$ and $3F_{200\ \mu s}$ deviates from the all Mn^{IV} assignment reported for S_3 and represented on our plot by MnO_2 oxide as well as two model compounds containing a single Mn^{IV} center. Intriguingly, the shift between $2F$ and $3F_{200\ \mu s}$ is greater than that observed between $2F$ and $3F_{500\ \mu s}$, for which

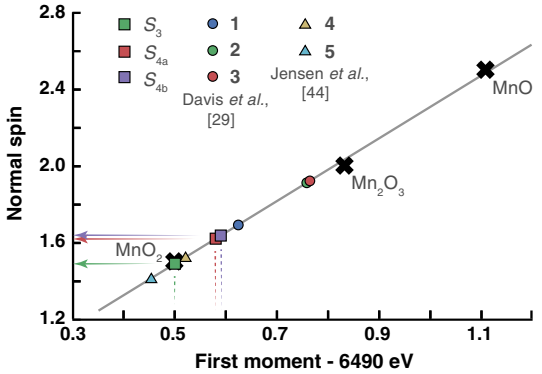

FIG. 4. Analysis of Mn $K\beta$ first moments. Placement of fully processed $2F$ and $3F$ data along a linear fit to a series of Mn oxide first moments empirically predicts the average spin state of Mn centers in the OEC. For reference, relevant Mn coordination complexes are placed along the line by using the nominal spins reported by Davis *et al.* and Jensen *et al.* [31,46]. Note that S_{4a} and S_{4b} correspond to $3F$ states with Δt between the final laser flash and an x-ray pulse of 50 and 200 μs, respectively. Compounds 1–3 are formally mixed valence Mn^{III}/Mn^{IV} complexes. 1 is a di-μ-oxo dimer, $[Mn_2O_2L'_4](ClO_4)_3$, while 2 and 3 are two examples from the Mn cubane family, $Mn_4O_4L_6$. Compounds 4 and 5, by contrast, are mononuclear Mn complexes $[Mn^{IV}(OH)_2(Me_2EBC)]^{2+}$ and $[Mn^{IV}(O)(OH)^-(Me_2EBC)]^+$, respectively.

statistical significance is visible only on some plots (Fig. 3) but is not strictly demonstrated in the 6.485–6.495 keV range. It is currently unclear whether this effect is rooted in statistical uncertainty or is simply a weak spectral change due to transient oxidation of the OEC by electron transfer to $Tyr_Z^\bullet$ (k_2) [Fig. 1(e)]. Transient oxidation would likely temporarily pause or reverse the reductive (increasing) trend in first moments.

While density functional theory (DFT) modeling has proven inconclusive regarding the formation of a $Mn^V{=}O$ species [24,26,49,50], we are unable to observe oxidation of the OEC, which would likely be associated with lower values of the first moment, at any observation time point following the third flash and measured over multiple beam times. This lack of evidence for oxidation past $2F$ (majority state S_3) is consistently observed (Figs. 3, S3, and S4 [5]) thereby excluding formation of a $Mn^VMn^{IV}{}_3$ state kinetic intermediate. Current DFT models [23–26] also do not resolve the previously identified kinetic challenge [22]. UV-vis difference spectra show that $Tyr_Z^\bullet$ is reduced quite slowly, approximately 1 ms after the third flash. Given that this time constant is comparable to the rate of O_2 evolution, only a very short approximately 50 μs time window remains for all bond-formation dynamics and product and substrate exchange to occur.

The TR XES results detailed above cannot be explained by most DFT mechanistic models. Those which propose a $Mn^{IV}{}_4 - O^\bullet$ (oxyl radical) in place of $Mn^V{=}O$, for

example, predict significant activation barriers for O—O bond formation [23,27], in disagreement with spectroscopic results that show early-onset reduction in both XES and XAS. Our results *are*, however, in agreement with the only other published TR studies probing the electronic structure evolution of the Mn centers via x-ray absorption spectroscopy (XAS) [3,4,18]. TR XAS detects no oxidation and, instead, suggests the gradual (milliseconds) reduction of the OEC, initiated 250 μs into the S_3-to-S_0 transition. In contrast to the XAS study, where only two energy points along the Mn K edge are analyzed, we collect full spectra with high multiplicity, representing the complete electronic structure of the OEC at $\Delta t \sim 50$ μs and $\Delta t \sim 200$ μs. In addition, XAS and XES probe different electronic transitions. It is therefore possible that some early spectral changes between $t = 0$–200 μs may have previously escaped detection or are less pronounced in XAS due to the transient nature of the early intermediate. A more recent XES study performed at the Linac Coherent Light Source indicates no changes to the Mn $K\beta$ spectra 250 μs after the third laser excitation [51]. We attribute this discrepancy to differences in experimental conditions that will likely be clarified in the future.

To overcome the kinetic challenge, we propose that the O—O formation step takes place in the S_3-to-S_0 transition prior to the reduction of $Tyr_Z^{\bullet}$ [Fig. 1(e)] [30,31]. Rapid evolution of the OEC during the S_3-to-S_0 transition has long been a primary target of PS II research. Based on UV-vis difference spectroscopy [17,52] and TR infrared spectroscopy [16], a deprotonation event is proposed to occur early (0–300 μs) during this transition. Our results do not explicitly exclude a deprotonation event but necessitate significant changes to the electronic structure of the 3d Mn frontier orbitals to explain the observed spectroscopic effect. The results presented here can be better rationalized if the formation of the $(Tyr_Z^{\bullet})S_3$ state, occurring on the order of 100 ns [16], triggers a sequence of events resulting in significant redox or structural changes to the OEC, such as the formation of the O—O bond. The most recent isotope exchange studies show that substrate exchange stops early (0–300 μs) in the transition [21], hinting at such a possibility. The highest activation energies are also noted in this early time window [53]. Likewise, the only molecularly defined system for water oxidation functioning with a comparative reaction rate $[Ru(bda)(isoq)_2]$ is hypothesized to work via a radical coupling mechanism, which results in a peroxo intermediate. During the final catalytic step of this artificial system, the peroxo intermediate is further oxidized, and release of O_2 follows [54]. These results suggest that the same catalytic mechanism engenders rapid O_2 evolution in both biological and biomimetic systems, while at the same time preventing peroxide release due to the transient presence of the peroxo isoform.

In summary, to analyze the evolution of the photosystem II electronic structure, we observed intermediate states of photosynthetic O_2 production via microsecond resolution time-resolved x-ray emission spectroscopy at a synchrotron source. Consistent with the obtained full spectra is a mechanism involving O—O bond formation in the S_3-to-S_0 transition prior to $Tyr_Z^{\bullet}$ reduction. This mechanism resolves the previously highlighted kinetic problems. Parallel advancements in the development of molecular catalysts for artificial photosynthesis strongly support O—O bond formation prior to the final oxidation step of such peroxo intermediates and provide further support for the mechanistic proposal detailed herein.

This research was supported by NSF, CHE-1350909 (Y. P.) and the NSF Graduate Research Fellowship under Grant No. DGE0833366 (K. D.). G. T. S. acknowledges support from the U.S. Department of Energy, Office of Science, under Grant No. DE-SC0002194. Use of the Advanced Photon Source, an Office of Science User Facility operated for the U.S. Department of Energy (DOE) Office of Science by Argonne National Laboratory, was supported by the U.S. DOE under Contract No. DE-AC02-06CH11357. Use of the BioCARS Sector 14 was also supported by the National Institutes of Health, National Institute of General Medical Sciences Grant No. 1R24GM111072. The time-resolved setup at BioCARS was funded in part through a collaboration with Philip Anfinrud (NIH/ NIDDK). We thank Professor L. Slipchenko from Purdue University for providing computational resources and helpful discussion.

[1] B. Kok, B. Forbush, and M. McGloin, *Cooperation of Charges in Photosynthetic Oxygen Evolution. I. A Linear Four Step Mechanism*, Photochem. Photobiol. **11**, 457 (1970).

[2] T. Wydrzynski and S. Satoh, *Photosystem II: The Light-Driven Water:Plastoquinone Oxidoreductase*, Advances in Photosynthesis and Respiration (Springer, Dordrecht, 2005).

[3] M. Haumann, P. Liebisch, C. Muller, M. Barra, M. Grabolle, and H. Dau, *Photosynthetic O_2 Formation Tracked by Time-Resolved X-Ray Experiments*, Science **310**, 1019 (2005).

[4] M. Haumann, A. Grundmeier, I. Zaharieva, and H. Dau, *Photosynthetic Water Oxidation at Elevated Dioxygen Partial Pressure Monitored by Time-Resolved X-Ray Absorption Measurements*, Proc. Natl. Acad. Sci. U.S.A. **105**, 17384 (2008).

[5] See Supplemental Material at http://link.aps.org/supplemental/10.1103/PhysRevX.8.041014 for expanded materials and methods.

[6] K. N. Ferreira, T. M. Iverson, K. Maghlaoui, J. Barber, and S. Iwata, *Architecture of the Photosynthetic Oxygen-Evolving Center*, Science **303**, 1831 (2004).

[7] A. Zouni, H. T. Witt, J. Kern, P. Fromme, N. Krauss, W. Saenger, and P. Orth, *Crystal Structure of Photosystem II from Synechococcus elongatus at 3.8 Å Resolution*, Nature (London) **409**, 739 (2001).

[8] A. Guskov, J. Kern, A. Gabdulkhakov, M. Broser, A. Zouni, and W. Saenger, *Cyanobacterial Photosystem II at 2.9-Å Resolution and the Role of Quinones, Lipids, Channels and Chloride*, Nat. Struct. Mol. Biol. **16**, 334 (2009).

[9] Y. Pushkar, J. Yano, P. Glatzel, J. Messinger, A. Lewis, K. Sauer, U. Bergmann, and V. Yachandra, *Structure and Orientation of the* Mn_4Ca *Cluster in Plant Photosystem II Membranes Studied by Polarized Range-Extended X-Ray Absorption Spectroscopy*, J. Biol. Chem. **282**, 7198 (2007).

[10] Y. Umena, K. Kawakami, J. R. Shen, and N. Kamiya, *Crystal Structure of Oxygen-Evolving Photosystem II at a Resolution of 1.9 Å*, Nature (London) **473**, 55 (2011).

[11] C. Glockner, J. Kern, M. Broser, A. Zouni, V. Yachandra, and J. Yano, *Structural Changes of the Oxygen-Evolving Complex in Photosystem II During the Catalytic Cycle*, J. Biol. Chem. **288**, 22607 (2013).

[12] C. Kupitz *et al.*, *Serial Time-Resolved Crystallography of Photosystem II Using a Femtosecond X-Ray Laser*, Nature (London) **513**, 261 (2014).

[13] M. Suga *et al.*, *Light-Induced Structural Changes and the Site of* O═O *Bond Formation in PSII Caught by XFEL*, Nature (London) **543**, 131 (2017).

[14] I. D. Young *et al.*, *Structure of Photosystem II and Substrate Binding at Room Temperature*, Nature (London) **540**, 453 (2016).

[15] K. M. Davis and Y. N. Pushkar, *Structure of the Oxygen Evolving Complex of Photosystem II at Room Temperature*, J. Phys. Chem. B **119**, 3492 (2015).

[16] T. Noguchi, H. Suzuki, M. Tsuno, M. Sugiura, and C. Kato, *Time-Resolved Infrared Detection of the Proton and Protein Dynamics during Photosynthetic Oxygen Evolution*, Biochemistry **51**, 3205 (2012).

[17] F. Rappaport, M. Blancharddesce, and J. Lavergne, *Kinetics of Electron-Transfer and Electrochromic Change during the Redox Transitions of the Photosynthetic Oxygen-Evolving Complex*, Biochim. Biophys. Acta-Bioenerg. **1184**, 178 (1994).

[18] I. Zaharieva, H. Dau, and M. Haumann, *Sequential and Coupled Proton and Electron Transfer Events in the* $S2 \rightarrow S3$ *Transition of Photosynthetic Water Oxidation Revealed by Time-Resolved X-Ray Absorption Spectroscopy*, Biochemistry **55**, 6996 (2016).

[19] I. Zaharieva, P. Chernev, G. Berggren, M. Anderlund, S. Styring, H. Dau, and M. Haumann, *Room-Temperature Energy-Sampling* $K\beta$ *X-Ray Emission Spectroscopy of the* Mn_4Ca *Complex of Photosynthesis Reveals Three Manganese-Centered Oxidation Steps and Suggests a Coordination Change Prior to* O_2 *Formation*, Biochemistry **55**, 4197 (2016).

[20] G. T. Babcock, R. E. Blankenship, and K. Sauer, *Reaction-Kinetics for Positive Charge Accumulation on Water Side of Chloroplast Photosystem*, FEBS Lett. **61**, 286 (1976).

[21] H. Nilsson, F. Rappaport, A. Boussac, and J. Messinger, *Substrate-Water Exchange in Photosystem II Is Arrested before Dioxygen Formation*, Nat. Commun. **5**, 4305 (2014).

[22] J. Kern and G. Renger, *Photosystem II: Structure and Mechanism of the Water:Plastoquinone Oxidoreductase*, Photosynth. Res. **94**, 183 (2007).

[23] P. E. M. Siegbahn, *Water Oxidation Mechanism in Photosystem II, Including Oxidations, Proton Release Pathways,* O─O *Bond Formation and* O_2 *Release*, Biochim. Biophys. Acta **1827**, 1003 (2013).

[24] T. Saito *et al.*, *Possible Mechanisms of Water Splitting Reaction Based on Proton and Electron Release Pathways Revealed for* $CaMn_4O_5$ *Cluster of PSII Refined to 1.9 Å X-Ray Resolution*, Int. J. Quantum Chem. **112**, 253 (2012).

[25] K. Yamaguchi *et al.*, *Full Geometry Optimizations of the Mixed-Valence* $Ca\,Mn_4O_4X(H_2O)(4)$ *(*X = Oh *or O) Cluster in Oec of PS II: Degree of Symmetry Breaking of the Labile* Mn─X─Mn *Bond Revealed by Several Hybrid Dft Calculations*, Int. J. Quantum Chem. **113**, 525 (2013).

[26] E. M. Sproviero, J. A. Gascon, J. P. McEvoy, G. W. Brudvig, and V. S. Batista, *Quantum Mechanics/Molecular Mechanics Study of the Catalytic Cycle of Water Splitting in Photosystem II*, J. Am. Chem. Soc. **130**, 3428 (2008).

[27] P. E. M. Siegbahn, O─O *Bond Formation in the* S_4 *State of the Oxygen-Evolving Complex in Photosystem II*, Chem. Eur. J. **12**, 9217 (2006).

[28] K. M. Davis *et al.*, *Fast Detection Allowing Analysis of Metalloprotein Electronic Structure by X-Ray Emission Spectroscopy at Room Temperature*, J. Phys. Chem. Lett. **3**, 1858 (2012).

[29] J. Kern *et al.*, *Simultaneous Femtosecond X-Ray Spectroscopy and Diffraction of Photosystem II at Room Temperature*, Science **340**, 491 (2013).

[30] K. M. Davis *et al.*, *Rapid Evolution of the Photosystem II Electronic Structure during Water Splitting*, arXiv:1506.08862.

[31] S. C. Jensen *et al.*, *X-Ray Emission Spectroscopy of Biomimetic Mn Coordination Complexes*, J. Phys. Chem. Lett. **8**, 2584 (2017).

[32] X.-c. Bai, G. McMullan, and S. H. W. Scheres, *How Cryo-Em Is Revolutionizing Structural Biology*, Trends Biochem. Sci. **40**, 49 (2014).

[33] P. Glatzel and U. Bergmann, *High Resolution 1s Core Hole X-Ray Spectroscopy in* 3*d Transition Metal Complexes—Electronic and Structural Information*, Coord. Chem. Rev. **249**, 65 (2005).

[34] K. M. Davis, I. Kosheleva, R. W. Henning, G. T. Seidler, and Y. Pushkar, *Kinetic Modeling of the X-Ray-Induced Damage to a Metalloprotein*, J. Phys. Chem. B **117**, 9161 (2013).

[35] B. A. Mattern, G. T. Seidler, M. Haave, J. I. Pacold, R. A. Gordon, J. Planillo, J. Quintana, and B. Rusthoven, *A Plastic Miniature X-Ray Emission Spectrometer (miniXES) Based on the Cylindrical Von Hamos Geometry*, Rev. Sci. Instrum. **83**, 023901 (2012).

[36] J. Messinger, W. P. Schroder, and G. Renger, *Structure-Function Relations in Photosystem-II—Effects of Temperature and Chaotropic Agents on the Period 4 Oscillation of Flash-Induced Oxygen Evolution*, Biochemistry **32**, 7658 (1993).

[37] J. Messinger *et al.*, *Absence of Mn-Centered Oxidation in the* S_2 *to* S_3 *Transition: Implications for the Mechanism of Photosynthetic Water Oxidation*, J. Am. Chem. Soc. **123**, 7804 (2001).

[38] Y. Pushkar, J. Yano, K. Sauer, A. Boussac, and V. K. Yachandra, *Structural Changes in the* Mn_4Ca *Cluster and the Mechanism of Photosynthetic Water Splitting*, Proc. Natl. Acad. Sci. U.S.A. **105**, 1879 (2008).

[39] R. Alonso-Mori *et al.*, *Towards Characterization of Photo-Excited Electron Transfer and Catalysis in Natural and Artificial Systems Using Xfels*, Faraday Discuss. **194**, 621 (2016).

[40] F. D. Fuller *et al.*, *Drop-on-Demand Sample Delivery for Studying Biocatalysts in Action at X-Ray Free-Electron Lasers*, Nat. Methods **14**, 443 (2017).

[41] T.-a. Ono, T. Noguchi, Y. Inoue, M. Kusunoki, T. Matsushita, and H. Oyanagi, *X-Ray Detection of the Period-Four Cycling of the Manganese Cluster in Photosynthetic Water Oxidizing Enzyme*, Science **258**, 1335 (1992).

[42] L. Iuzzolino, J. Dittmer, W. Dörner, W. Meyer-Klaucke, and H. Dau, *X-Ray Absorption Spectroscopy on Layered Photosystem II Membrane Particles Suggests Manganese-Centered Oxidation of the Oxygen-Evolving Complex for the* $S_0 - S_1$, $S_1 - S_2$, *and* $S_2 - S_3$ *Transitions of the Water Oxidation Cycle*, Biochemistry **37**, 17112 (1998).

[43] M. Haumann, C. Muller, P. Liebisch, L. Iuzzolino, J. Dittmer, M. Grabolle, T. Neisius, W. Meyer-Klaucke, and H. Dau, *Structural and Oxidation State Changes of the Photosystem II Manganese Complex in Four Transitions of the Water Oxidation Cycle* ($S-0 \rightarrow S-1$, $S-1 \rightarrow S-2$, $S-2 \rightarrow S-3$, *and* $S-3$, $S-4 \rightarrow S-0$) *Characterized by X-Ray Absorption Spectroscopy at 20 K and Room Temperature*, Biochemistry **44**, 1894 (2005).

[44] N. Cox, M. Retegan, F. Neese, D. A. Pantazis, A. Boussac, and W. Lubitz, *Electronic Structure of the Oxygen Evolving Complex in Photosystem II Prior to* O─O *Bond Formation*, Science **345**, 804 (2014).

[45] N. Schuth, I. Zaharieva, P. Chernev, G. Berggren, M. Anderlund, S. Styring, H. Dau, and M. Haumann, Kα *X-Ray Emission Spectroscopy on the Photosynthetic Oxygen-Evolving Complex Supports Manganese Oxidation and Water Binding in the S3 State*, Inorg. Chem. **57**, 10424 (2018).

[46] K. M. Davis, M. C. Palenik, L. Yan, P. F. Smith, G. T. Seidler, G. C. Dismukes, and Y. N. Pushkar, *X-Ray Emission Spectroscopy of Mn Coordination Complexes Towards Interpreting the Electronic Structure of the Oxygen Evolving Complex of Photosystem II*, J. Phys. Chem. C **120**, 3326 (2016).

[47] G. Vanko, T. Neisius, G. Molnar, F. Renz, S. Karpati, A. Shukla, and F. M. F. de Groot, *Probing the* 3*d Spin Momentum with X-Ray Emission Spectroscopy: The Case of Molecular-Spin Transitions*, J. Phys. Chem. B **110**, 11647 (2006).

[48] Y. Pushkar, K. M. Davis, and M. C. Palenik, *Model of the Oxygen Evolving Complex Which Is Highly Predisposed to* $O-O$ *Bond Formation*, J. Phys. Chem. Lett. **9**, 3525 (2018).

[49] S. Yamanaka *et al.*, *Structure and Reactivity of the Mixed-Valence* $CaMn_4O_5(H_2O)(4)$ *and* $CaMn_4O_4(OH)(H_2O)(4)$ *Clusters at Oxygen Evolution Complex of Photosystem II. Hybrid Dft (UB3LYP and UBHandHLYP) Calculations*, Int. J. Quantum Chem. **112**, 321 (2012).

[50] S. Yamanaka *et al.*, *Possible Mechanisms for the* O─O *Bond Formation in Oxygen Evolution Reaction at the* $CaMn_4O_5(H_2O)(4)$ *Cluster of PSII Refined to 1.9 Å X-Ray Resolution*, Chem. Phys. Lett. **511**, 138 (2011).

[51] J. Kern *et al.*, *Taking Snapshots of Photosynthetic Water Oxidation Using Femtosecond X-Ray Diffraction and Spectroscopy*, Nat. Commun. **5**, 4371 (2014).

[52] M. Haumann, O. Bogershausen, D. Cherepanov, R. Ahlbrink, and W. Junge, *Photosynthetic Oxygen Evolution: H/D Isotope Effects and the Coupling between Electron and Proton Transfer During the Redox Reactions at the Oxidizing Side of Photosystem II*, Photosynth. Res. **51**, 193 (1997).

[53] H. Bao and R. L. Burnap, *Structural Rearrangements Preceding Dioxygen Formation by the Water Oxidation Complex of Photosystem II*, Proc. Natl. Acad. Sci. U.S.A. **112**, E6139 (2015).

[54] L. Duan, F. Bozoglian, S. Mandal, B. Stewart, T. Privalov, A. Llobet, and L. Sun, *A Molecular Ruthenium Catalyst with Water-Oxidation Activity Comparable to That of Photosystem II*, Nat. Chem. **4**, 418 (2012).